Inverse Modeling of Seasonal Variations in the North Atlantic Ocean

LISAN YU* AND PAOLA MALANOTTE-RIZZOLI

Center for Meteorology and Physical Oceanography, Department of Earth, Atmospheric, and Planetary Sciences, Massachusetts Institute of Technology, Cambridge, Massachusetts

(Manuscript received 11 October 1996, in final form 25 August 1997)

ABSTRACT

An ocean general circulation model (OGCM) of the North Atlantic Ocean is fitted to the monthly averaged climatological temperatures and salinities of Levitus using the adjoint method, representing a significant step forward with respect to previous steady OGCM assimilations. The inverse approach has two important advantages over purely prognostic calculations: (i) it provides an estimate of the North Atlantic circulation and of its seasonal variability, which is optimally consistent with the OGCM dynamics and with the assimilated hydrography; (ii) it provides optimal estimates of the monthly surface heat and freshwater fluxes consistent with the used climatology, which are the most poorly known surface forcing functions.

Seasonality is ensured by penalizing field differences between month 13 and month 1 of the forward time integration within each iteration of the adjoint procedure. The primary goal of this work is to estimate large-scale oceanic properties important for climate issues and how they are affected by the inclusion of the seasonal cycle. The resultant meridional overturning displays significant seasonal variations. The surface Ekman cell centered at 35°N reaches a maximum intensity of ~7 Sv (Sv $\equiv 10^6$ m^3 s^{-1}) in wintertime, while the North Atlantic Deep Water cell reaches a maximum strength of ~19 Sv in summertime. Its annual average is of ~17 Sv, in good agreement with the recent estimate of Schmitz and McCartney. The poleward heat transport exhibits the strongest seasonal variations, reaching its maximum value of 0.85×10^{15} W at ~25°N in summertime or 0.85 PW (1 PW = 10^{15} W). The annual average at 25°N is ~0.7 PW, weaker than observational estimates. The dynamical analysis indicates that the wind forcing is the controlling factor for these variations by controlling the time-varying Ekman cell.

Comparison with previous steady-state optimizations of Yu and Malanotte-Rizzoli shows that the optimization with seasonal forcing produces three major improvements in the inverse results. First, the inclusion of the seasonal cycle greatly improves the estimated hydrography (temperature and salinity fields) by eliminating the basinwide cold bias in the upper ocean and the warm bias in the deep ocean found in the steady-state inversions. As a consequence, the velocity fields are also significantly improved, with a tight and strong Gulf Stream jet.

Second, the monthly optimal estimates of surface heat and freshwater fluxes provide an annual average resembling closely the observational climatological means, a striking contrast to the fluxes estimated in the steady assimilation.

Finally, the most important improvement is in the estimate of the poleward heat transport. The annual mean meridional heat transport shows an increase of ~0.2 PW at all latitudes with respect to the steady-state heat transport, thus demonstrating the importance of rectification effects of the seasonal cycle.

1. Introduction

Modeling the large-scale ocean general circulation and hydrographic structures using oceanic general circulation models (OGCMs) and the adjoint assimilation technique has progressed rapidly in recent years (e.g., Tziperman et al. 1992a,b; Marotzke and Wunsch 1993; Bergamasco et al. 1993; Sirkes and Tziperman 1995; Schiller 1995; Yu and Malanotte-Rizzoli 1996). The adjoint OGCM approach has major advantages over purely prognostic calculations in combining various observational datasets into one dynamical framework, in systematically testing the model's consistency with existing data, and in providing information for improving model formulation and parameterizations. One of the major goals of the adjoint inverse modeling is to produce an ocean state with model–data consistency for climate diagnostic studies and for better climate predictions.

Many attempts have been made with adjoint OGCMs to search for a steady ocean estimate with model–data consistency to describe the North Atlantic large-scale mean ocean general circulation and hydrography. However, these experiments have produced steady-state circulations that satisfy a priori observational error esti-

* Current affiliation: Joint Center for Earth System Sciences/Department of Meteorology, University of Maryland, College Park, Maryland.

Corresponding author address: Dr. Lisan Yu, Joint Center for Earth System Sciences/Dept. of Meteorology, University of Maryland, College Park, MD 20742.
E-mail: lyu@atmos.umd.edu

mates only marginally (Tziperman et al. 1992b; Marotzke and Wunsch 1993; Schiller 1995; Yu and Malanotte-Rizzoli 1996). In particular, these experiments have all encountered a systematic surface cold bias in the optimal solution. The departure of the steady optimal surface temperature from the yearly climatology can be as large as 6°–8°C in some regions (e.g., Yu and Malanotte-Rizzoli 1996), corresponding to the yearly variability due to seasonal cycle. This result demands a reexamination of the steady-state concept and/or the model formulation regarding the mechanism(s) responsible for the large temperature deficiency.

Yu and Malanotte-Rizzoli (1996, hereafter YM96) in a recent study have found that this surface cold bias reflects just part of the systematic error pattern in the vertical—the model has at the same time a warm bias in the deep ocean. YM96 analysis indicates that the cold surface layer is a correction imposed by the optimization to reduce large data misfits in the deep ocean resulting from a deep ocean warming. The appearance of the deep warming is due to the use of the steady-state assumption and the annual mean climatology and due to the limitation of the model's northern boundary condition. Since the model has a limited domain, a rigid wall is imposed at the northern boundary where a buffer zone is inserted to relax the modeled temperature and salinity toward climatological values. By doing so, the modeled deep waters are formed through an artificial sinking process in the buffer zone, and the deep water characteristics are therefore determined by the properties of the surface water in the sinking region. Without the seasonal cycle, the deep water is produced from sinking surface water with the annual mean temperature. However, the annual mean hydrography has a surface water warmer than the observed winter surface water. This inevitably leads to a warmer deep ocean and large model–data discrepancies in the vast deep layer. In order to reduce the misfits as required by the optimal procedure, the model's deep water source, that is, the surface layer, has to be made cooler. Therefore, the systematic surface cooling compensates for the deep warming and is the outcome of the least squares requirement for an optimal model–data fitting in a three-dimensional space. The YM96 study suggests that a better simulation of the three-dimensional hydrography requires at least the inclusion of the seasonal cycle.

This study therefore capitalizes on the seasonal variability of the North Atlantic circulation by fitting an OGCM to the monthly averaged climatological temperatures and salinities of Levitus (1994a,b) using the adjoint method. Inclusion of the seasonal cycle is straightforward in purely prognostic calculations by including seasonal variability in the surface forcing function (wind stress) and surface boundary conditions for temperature and salinity, that is, relaxation to surface monthly climatologies in the vast majority of simulations. Inclusion of the seasonal cycle in the adjoint OGCM, on the other hand, is not straightforward, as will be discussed in section 2.

TABLE 1. Parameters used in the study.

Horizontal viscosity	$A_h = 1.0 \times 10^9$ cm^2 s^{-1}
Vertical viscosity	$A_v = 1.0 \times 10^7$ cm^2 s^{-1}
Horizontal diffusivity	$K_h = 10$ cm^2 s^{-1}
Vertical diffusivity	$K_v = 0.3$ cm^2 s^{-1}
Time step	$\Delta t = 1$ h
Horizontal resolution	$\Delta\phi = 2°$, $\Delta\lambda = 1.2°$

A variety of prognostic calculations have been recently carried out in the North Atlantic following the Community Modeling Effort (CME) initiated by Bryan and Holland. Most of these studies have focused on investigating the effect of increased horizontal resolution, and hence of resolving mesoscale eddy variability, on the simulation of the North Atlantic circulation (Beckmann et al. 1994a,b; Klinck 1995). These studies have also identified deficiencies of prognostic models, such as the northward overshooting of the Gulf Stream jet, which is common for coarse resolution simulations. The effect of the seasonal cycle has also been investigated but mostly in the context of medium to high resolutions (Böning et al. 1991; Böning and Herrmann 1994). The comparison of the above prognostic model results with ours is however meaningless in view of the quite different horizontal resolution of our simulations, not eddy resolving (2° lat by 1.2° long).

The prognostic calculations closest to ours are those carried out in the CME effort with coarse horizontal resolution of 1.2° lat by 1° long, discussed by Holland and Bryan (1994). They carry out a thorough sensitivity study of the North Atlantic circulation within a domain between 15°S and 65°N, hence rather more extended in latitude than ours (see following sections). Sensitivity experiments are discussed with respect to a baseline calculation, their experiment 12, by changing northern and southern boundary conditions, surface forcing functions (wind, salt flux patterns), initial conditions, and open versus closed boundaries. In their Table 1, they summarize the results by comparing the two integral quantities of greatest climate relevance, that is, the total meridional overturning of North Atlantic Deep Water and the maximum northward heat transport near 25°N in whatever season it does occur. The baseline experiment 12 produces 16.6 Sv (Sv $\equiv 10^6$ m^3 s^{-1}) of meridional overturning and a maximum heat transport of 0.7 PW. Both quantities exhibit a wide range of variations. The meridional overturning changes from the minimum of 0.2 Sv (different initial conditions) to the maximum of 23.8 Sv (salt flux pattern diminished at north). The maximum heat transport also exhibits large variations, from a minimum of 0.21 PW (different initial conditions) to a maximum of 1.09 PW (open boundaries plus isopycnal mixing). The wide ranges of these estimates demonstrate the extreme sensitivity of prognostic

calculations to often minor changes in the experiment configuration.

Böning et al. (1995) also compare different experiments of the CME effort differing in horizontal resolution, coarse to eddy resolving; wind and thermohaline forcing; and mixing parameterizations. In the standard case of 1.2° lat by 1° long the meridional overturning transport is 16 Sv, that is, realistic, but the meridional heat transport at 25°N is ~0.6 PW. They explain this deficiency in the heat transport estimate, in spite of the realistic NADW formation rate, due to the shortcut of the NADW thermohaline cell produced by a strong upwelling region between 30° and 40°N in the western boundary layer. This artificial upwelling strongly reduces the meridional heat transport and is a result of the use of the traditional horizontal eddy diffusivity coefficient (Veronis 1975; Cummins et al. 1990). The spurious upwelling is in fact eliminated by using the isopycnal mixing scheme of Gent and McWilliams (1990). In the following sections we shall contrast these prognostic model results with our inverse ones wherever meaningful.

We use the Bryan–Cox primitive equation model and its exact adjoint model to simulate the seasonal variations of the North Atlantic Ocean. It should be emphasized that, although the adjoint inversion of the seasonal climatology has been already carried out with a simple tropical ocean model (Yu and O'Brien 1995), the published literature on the adjoint OGCMs have not yet exceeded the framework of the steady-state circulation. Therefore, this work represents a significant step forward with respect to steady-state adjoint inversions.

The adjoint OGCM in use was constructed by Yu and Malanotte-Rizzoli (1995, 1996) from the original prototype made at the Atlantic Oceanographic and Meteorological Laboratory (Long et al. 1989, unpublished manuscript). This adjoint version differs from the one used by Tziperman et al. (1992a,b) or Marotzke and Wunsch (1993) in the model dynamics: we use the complete full-nonlinear primitive equations, whereas Tziperman et al. or Marotzke and Wunsch use a planetary geostrophic relation of the momentum equations. The results from YM96 have demonstrated the advantage of using the full OGCM dynamics and its exact adjoint in that the full nonlinear model can simulate a better frontal structure of the Gulf Stream system and smoother large-scale features of the velocity fields. This adjoint model is also different from the one implemented by Schiller (1995): we follow the exact adjoint formulation proposed by Thacker and Long (1988), while Schiller adopts an approximate approach in which his adjoint model lacks the adjoint momentum equations.

The paper is organized as follows. Section 2 gives a brief description of the model, the data, and the adjoint procedure. The optimality of the solution is discussed in section 3. Section 4 analyzes the results, with emphasis on the seasonal variability of the model dynamical evolution. The comparisons between the mean states from the annual average of this study together with the steady-state patterns from the previous inversion of YM96 are discussed in section 5. Summary and conclusions are given in section 6.

2. The adjoint assimilation

The adjoint method has received great attention in recent years as it is feasible for applications to large systems. Since there have been many research papers discussing the adjoint theory and applications, we will not provide the detailed methodology here. Readers are referred to the studies by Le Dimet and Talagrand (1986), Thacker and Long (1988), Daley (1990), and Ghil and Malanotte-Rizzoli (1991) for theoretical guidance or the studies by Tziperman et al. (1992a,b), Marotzke and Wunsch (1993), Bergamasco et al. (1993), Sirkes and Tziperman (1995), Schiller (1995), and Yu and Malanotte-Rizzoli (1996) for pertaining technical questions. In the following only a brief description about the data, the model, and the cost function used in this study is given.

a. Dynamical model

The numerical model of the wind-driven and thermohaline circulation based on the primitive equations was developed by Bryan (1969) and Cox (1984). The essential assumptions of the model are the hydrostatic assumption, the Boussinesq approximation, and a closure approximation for small-scale motions based on the turbulent viscosity hypothesis. The governing continuous equations are

$$\mathbf{u}_t + \mathbf{u}\cdot\nabla_h\mathbf{u} + w\mathbf{u}_z + f\mathbf{k}\times\mathbf{u} = -\frac{1}{\rho_0}\nabla_h p + A_v\mathbf{u}_{zz} + A_h\nabla_h^2\mathbf{u}, \quad (1)$$

$$p_z + \rho g = 0, \quad (2)$$

$$\nabla_h\cdot\mathbf{u} + w_z = 0, \quad (3)$$

$$\rho = \rho(T, S, p), \quad (4)$$

$$(T,S)_t + \mathbf{u}\cdot\nabla_h(T,S) + w(T,S)_z = K_v(T,S)_{zz} + K_h\nabla_h^2(T,S), \quad (5)$$

with the surface boundary condition

$$w = 0, \qquad A_v\mathbf{u}_z = \tau/\rho_a, \qquad K_v(T, S)_z = (Q_T, S_0Q_S), \quad (6)$$

and the bottom condition

$$w = -\mathbf{u}\cdot\nabla_h H, \qquad A_v\mathbf{u}_z = 0, \qquad K_v(T, S)_z = 0. \quad (7)$$

Here $\mathbf{u}$ is the horizontal velocity vector with components (u, v) in the zonal (λ) and meridional (ϕ) directions and w the vertical velocity; p, ρ, g, and f are the pressure, the density, the acceleration of gravity, and the Coriolis parameter; $\mathbf{k}$ is a unit vector in the vertical (z)

TABLE 2. Vertical distribution of the standard errors. Here z_k^{TS} is the depth of a *u, v, T, S* grid point; $\langle \sigma_{T,k} \rangle$ is the horizontally averaged standard error for temperature; and $\langle \sigma_{S,k} \rangle$ is the horizontally averaged standard error for salinity. These error estimates are interpolated from the Levitus (1994a,b) climatology.

Level k	z_k^{TS}	$\langle \sigma_{T,k} \rangle$	$\langle \sigma_{S,k} \rangle$
1	25.0	1.397	0.333
2	75.0	1.260	0.210
3	150.0	1.050	0.160
4	250.0	0.860	0.130
5	350.0	0.760	0.126
6	450.0	0.701	0.120
7	550.0	0.639	0.115
8	650.0	0.584	0.109
9	750.0	0.535	0.110
10	850.0	0.488	0.111
11	950.0	0.459	0.105
12	1100.0	0.430	0.100
13	1350.0	0.395	0.101
14	1650.0	0.354	0.0869
15	2000.0	0.330	0.0900
16	2400.0	0.300	0.0837
17	2800.0	0.248	0.0623
18	3250.0	0.194	0.0392
19	3750.0	0.141	0.0187
20	4250.0	0.0853	0.0083
21	4750.0	0.0658	0.0105
22	5250.0	0.0789	0.0098

direction and ∇_h the horizontal gradient operator in spherical coordinates; A_v and A_h the vertical and horizontal eddy viscosity coefficients; (T, S) stand for the potential temperature and the salinity; and K_v and K_h are the vertical and horizontal diffusivities of heat and salt. Convective overturning is simulated by homogenizing adjacent levels when they become statically unstable with respect to each other. The surface wind stress, heat flux, and freshwater flux (defined as evaporation minus precipitation) are denoted by τ, Q_T, and Q_S. The values of the most important model parameters used in the study are listed in Table 1.

The discretized form for the above equations (1)–(7) can be generalized as

$$\mathcal{X}_{ijk}^n = \mathcal{F}_n(\mathcal{X}_{ijk}^{n-1}, Q_{Tij}^{n-1}, Q_{Sij}^{n-1}) \qquad n = 1, 2, \cdots, N_T, \quad (8)$$

where (ijk) represents the grid location, $\mathcal{X}_{ijk}^n = (\mathbf{u}_{ijk}^n, T_{ijk}^n, S_{ijk}^n, \psi_{ijk}^n)^{\mathrm{T}}$ is a vector of the model prognostic variables at time step n, and $()^{\mathrm{T}}$ denotes the transpose. The total integration time is denoted by N_T. For convenience, we will use the model discretized form (8) in the following sections.

The North Atlantic ocean model, which has the same model configuration as that of YM96, extends from 9°N to 65°N, 100°W to 0°. The resolution is 1.2° long and 2° lat with 22 levels in the vertical (see Table 2 for the level distribution). Realistic topography and coastline are implemented. At the model northern and southern boundaries, buffer zones of six-degree width are introduced where the temperatures and salinities computed from the model are restored to observed values by a damping term, $\gamma(T - T^*)$ and $\gamma(S - S^*)$, respectively. The damping timescale ($1/\gamma$) is 30 days. Linear interpolation between the monthly climatological values is used for the reference temperature T^* and salinity S^*. A similar buffer zone is also inserted near the Mediterranean Sea outflow region (in the depths between 900 and 2400 m) but with a damping timescale of 360 days. For simplicity, each model month is specified to be 30 days.

b. Data

Monthly mean climatological data are used for the study, The wind stress fields are taken from the Hellerman and Rosenstein (1983) climatology and are the forcings for driving the momentum equations. They remain unchanged during the optimization. The temperature and salinity monthly mean distributions are from the Levitus (1994a,b) new climatology; they are the data used for the adjoint assimilation. The Oberhuber (1988) monthly surface heat and freshwater fluxes are not involved in the assimilation, but are used as the first guess field for starting the iterative adjoint procedure and later as a reference to compare with the optimally estimated fluxes. The climatological data are all interpolated onto model spatial grid by a cubic-spline scheme.

Error estimates of the Levitus hydrography climatology are needed in the adjoint calculations. However, three-dimensional error structures of the hydrographic fields are hardly available, not to mention the time variance of these structures. So we rely on the Levitus (1994a,b) horizontally averaged time-mean standard error estimates for the North Atlantic hydrographic fields and construct the mean error profiles for temperature and salinity (see Table 2). The error estimates for current velocities are the same as in YM96, which range from 2.5 cm s^{-1} at the surface down to 0.2 cm s^{-1} near the bottom. They were taken from measurements carried out at an extended mooring array in the Gulf Stream system near 55°W by Hogg (1994).

c. Cost function

In the adjoint procedure, the differences between data and the corresponding model components are formulated in a cost function by using a least squares formalism. The computations are to search values of the model's inputs (e.g., the initial conditions, the boundary conditions, and model unknown parameters such as the various mixing coefficients) that give the best model–data comparison. The model inputs we want to estimate in this study are the model initial state and the upper thermal and haline boundary conditions, or more specifically, the monthly surface heat and freshwater fluxes. The objective is to find optimal values of these model fields so that the model agrees with the Levitus monthly hydrography within the accuracy of the prespecified error estimates. The cost function is then defined as

$$\mathcal{J} = \underbrace{\frac{1}{2}\sum_{m}\sum_{i,j,k}\left[W_k^T(T_{ijk,m} - T_{ijk,m}^{\text{obs}})^2 + W_k^S(S_{ijk,m} - S_{ijk,m}^{\text{obs}})^2\right]}_{\text{I}}$$

$$+ \underbrace{\frac{1}{2}\sum_{p}\sum_{i,j,k}\left[W_k^T(T_{ijk,13}^p - T_{ijk,1}^p)^2 + W_k^S(S_{ijk,13}^p - S_{ijk,1}^p)^2 + W_k^{\mathbf{u}}(\mathbf{u}_{ijk,13}^p - \mathbf{u}_{ijk,1}^p)^2\right]}_{\text{II}}, \tag{9}$$

where the index (i, j, k) denotes the model grid position. The terms in group I represent the misfits between the modeled and the climatological temperatures and salinities and are calculated at the 15th day of each month, so m spans over the 12 model months. The seasonality is ensured by adding the terms in group II, which penalize the field differences between the month 13 and month 1. The index p denotes how frequent the fields at these two months are compared. We use $p = 3$, meaning that the field differences are calculated three times at days 5, 15, and 25.

The W_k^T, etc., in (9) are the weighting coefficients. Based upon the error estimates provided in the previous subsection, those weights can be calculated as follows:

$$W_k^T = \frac{\langle\sigma_{Tk}\rangle^{-2}}{N3}, \qquad W_k^S = \frac{\langle\sigma_{Sk}\rangle^{-2}}{N3}, \qquad W_k^{\mathbf{u}} = \frac{\langle\sigma_{\mathbf{u}k}\rangle^{-2}}{N3}, \tag{10}$$

where $\langle\sigma_{Tk}\rangle$ and $\langle\sigma_{Sk}\rangle$ are the horizontal mean errors of climatological temperature and salinity fields at level k and $\langle\sigma_{\mathbf{u}k}\rangle$ is the horizontal error estimates of the velocity fields at level k; $N3$ is the total number of the 3D grid points. The seasonality penalties for temperature and salinity fields (terms in group II) use the same weighting coefficients as specified in (10).

The cost formulation (9) differs from the one used in YM96 in two major aspects. Whereas YM96 considers the steady circulation and so its cost function includes the steady constraints to penalize the temporal derivatives, this study concerns the seasonal variability of the ocean and therefore the steady constraints are removed. But we include the terms of group II to ensure the seasonality in the adjoint calculations. The second difference lies in the number of the estimated parameters. YM96 determines the steady surface flux fields, while this study estimates the monthly flux fields. By doing so, the number of the estimated parameters is about 12 times larger than that of YM96. Note that the estimation of the monthly flux fields is not constrained in (9) since YM96 as well as other studies have found that including the flux constraints in the cost function makes the adjoint procedure difficult to converge due to the large inconsistency between the fluxes and the hydrographic climatologies.

d. Adjoint procedure

The problem of finding a minimum of the cost function (9) while satisfying the model equation (8) is the problem of a constrained minimization and needs to be transformed into an unconstrained problem. This can be done by formulating a Lagrange function that combines the cost function and the model equations through the Lagrange multipliers. By using the Sasaki (1970) ''strong'' constraint formalism, the Lagrange function takes the form

$$\mathcal{L} = \mathcal{J} + \sum_{n}\sum_{ijk}\lambda_{ijk}^n[\mathcal{X}_{ijk}^n - \mathcal{F}_n(\mathcal{X}_{ijk}^{n-1}, \mathcal{Q}_{Tij}^{n-1}, \mathcal{Q}_{Sij}^{n-1})]. \tag{11}$$

The following equations, which require the first-order variation of $\mathcal{L}$ to vanish, result from the condition of finding the stationary points of (11):

$$\frac{\partial\mathcal{L}}{\partial\lambda_{ijk}^n} = 0 \Rightarrow \mathcal{X}_{ijk}^n = \mathcal{F}_n(\mathcal{X}_{ijk}^{n-1}, \mathcal{Q}_{Tij}^{n-1}, \mathcal{Q}_{Sij}^{n-1}) \quad \text{[recovering the model Eq. (8)]} \tag{12}$$

$$\frac{\partial\mathcal{L}}{\partial\mathcal{X}_{ijk}^n} = 0 \Rightarrow \lambda_{ijk}^n = \left[\frac{\partial\mathcal{F}_{n+1}}{\partial\mathcal{X}_{ijk}^n}\right]^T\lambda_{ijk}^{n+1} - \frac{\partial\mathcal{J}}{\partial\mathcal{X}_{ijk}^n} \quad \text{(resulting in the adjoint model)} \tag{13}$$

$$\frac{\partial\mathcal{L}}{\partial\mathcal{Q}_{lij}^m} = \frac{\partial\mathcal{J}}{\partial\mathcal{Q}_{lij}^m} + \sum_{n}^{M_T}\left[\frac{\partial\mathcal{F}_n}{\partial\mathcal{Q}_{lij}^m}\right]^T\lambda_{ij,k=1}^n \Rightarrow \begin{cases} = 0 & \text{minimum} \\ \neq 0 & \text{gradient of } \mathcal{J} \text{ w.r.t. } \mathcal{Q}_l, \end{cases} \tag{14}$$

where $l = T, S$

$$\frac{\partial\mathcal{L}}{\partial\mathcal{X}_{ijk}^{n=0}} = \frac{\partial\mathcal{J}}{\partial\mathcal{X}_{ijk}^{n=0}} + \lambda_{ijk}^{n=0} \Rightarrow \begin{cases} = 0 & \text{minimum} \\ \neq 0 & \text{gradient of } \mathcal{J} \text{ w.r.t. } \mathcal{X}_{ijk}^{n=0}. \end{cases} \tag{15}$$

Since only monthly flux patterns are estimated, the flux values at each time during the model integration are given by the linear interpolation between monthly values. So the summation in (14) is made over M_T, the total integration time of the month m, to accumulate the distributed flux effects.

The system (12)–(15) is solved iteratively in search for a minimum. The procedure is carried out in the following order:

Step 1. Choose the first guess values for the model inputs of initial field $X^{n=0}$ and the monthly surface fluxes Q_T and Q_S. In this study, the guess field for the model initial state is taken from the final state of the model's 10-yr spinup, and the guess field for the surface fluxes is specified to be the Oberhuber (1988) flux climatology. The 10-yr spinup run is initialized with the Levitus (1994a,b) January hydrography and uses the surface relaxation scheme for both temperature and salinity. The relaxation timescale is 30 days. The model parameters and side boundary conditions are the same as those stated in section 2a.

Step 2. Integrate the model equation (12) forward for 13 months by using the given model inputs. The integration strategy of 13 months is to ensure the seasonality to be maintained within each iteration. The model field information at days 5, 15, 25 of each month is saved for the adjoint model integration. If the computational resources permitted, the model field should be saved at every single integration time. But this is not possible for a large model such as the OGCM. Linear interpolation between 10-day fields is used to project the information onto each adjoint model integration time. Considering the timescale of the study is the annual cycle, such interpolation is not detrimental to the modeled seasonal variability.

Step 3. Calculate the gradient of the data misfits (terms in group I) at every 15th day to be used as the forcings in the adjoint model. The forcings at all the other times are set to zero. Then integrate the adjoint model (13) backward in time.

Step 4. Based on (14) and (15), calculate the gradient $\mathcal{J}$ with respect to controls $X^{n=0}|_\nu$, $Q_T|_\nu$, and $Q_S|_\nu$, where ν is the iteration number. Check to see if the convergence criteria are satisfied. If not, go on to the next step. Otherwise, stop the procedure. In this study, two criteria are used to control the procedure: (i) the initialized L_2 norm of the gradient is of $O(10^{-2})$ and (ii) the change of the cost value during the last 15 iterations is of $O(10^{-4})$. Note that when the procedure converges, the cost function is at a minimum for a linear problem, but is not always the case for a nonlinear problem—the cost function can be at any stationary point (i.e., a local minimum or a saddle point). Discussion of the optimality of the solution obtained in this study is given in the next section.

Step 5. Update the control variables using the formula: $C|_{\nu+1} = C|_\nu + \beta \mathbf{d}|_{\nu+1}$, where $C = X^{n=0}$, Q_T, and Q_S.

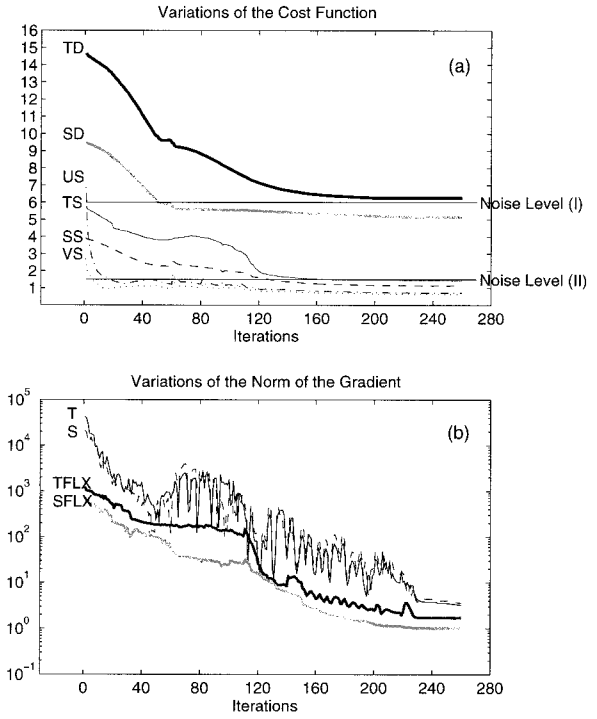

FIG. 1. The variations of (a) the cost function and (b) the norm of the gradient during the optimization. The procedure is terminated after 260 iterations. Here, TD and SD denote the temperature and salinity data misfit, respectively; TS, SS, US, and VS are the seasonal steady penalty of temperature, salinity, and longitudinal and meridional component of the velocity, respectively.

The optimal step-size β is estimated by using the scheme of Derber (1987), which requires an additional run of the forward OGCM. The search direction $\mathbf{d}|_{\nu+1}$ is computed by a conjugate gradient method (Navon and Legler 1987). Go to Step 2.

One can see that each iteration of the adjoint procedure involves three model integrations with the size of an OGCM: one to compute the forward OGCM to determine the solution (step 2), one to compute the adjoint OGCM (step 4) for calculating the gradients, and one to compute the forward OGCM to determine the step size (step 5). That an adjoint OGCM is computationally expensive lies in two aspects: the long computation time and the large storage requirement. The former is due to the fact that several hundred iterations are needed to obtain an optimal solution. The latter arises because of the requirement for the frequent recording of the field information during the forward model run.

3. Optimality of the solution

The experiment is conducted following the procedure outlined in section 2c. The variations of each cost term and the norm of the gradient with iterations are displayed in Fig. 1. The plot shows that the temperature and salinity data misfit terms are the major terms in the

cost function, and the seasonality penalty terms make rather small contributions. It also shows that all the cost terms have a fast reduction during the first 150 iterations and a slow adjustment for the rest of the minimization. The iterative process is terminated after iteration 260, at which the solution achieves the computationally steady state and satisfies the two criteria for convergence (i.e., the changes in either the cost values or the norms of the gradient are insignificant).

The necessary conditions for a solution to be optimal require that (i) the data constraints and the seasonality penalties obtain a compromise with each other and (ii) they satisfy the preassumed error estimates. These conditions define that each individual cost term at the solution should be equally large and should be of the magnitude of 0.5. Considering that the terms in group I in cost function (9) are the sum of the misfits over 12 months and the terms in group II are the accumulation of the field differences at days 5, 15, and 25 between month 13 and month 1, it is expected that the optimal value should be around 6.0 for each term in group I and 1.5 for each term in group II. These values are also referred to as the noise levels (see Fig. 1). At the final solution, the contributions from temperature and salinity data misfit are 6.25 and 5.14 respectively, and the contributions from the seasonality misfit of temperature, salinity, and velocity components u and v are respectively to be 1.42, 1.14, 0.72, and 0.64. Obviously all the seasonality terms are in the same order of magnitude and fall below the noise level as is seen from Fig. 1. The salinity data misfit is well within the preassumed error bar, but the temperature data misfit is slightly higher than what is expected. However, the deviation is very small, so it is fair to say that the two conditions for the optimality are reasonably satisfied.

4. Seasonal variability in the North Atlantic Ocean

a. Horizontal velocity fields, meridional circulations, and poleward heat transport

Until now quantitative descriptions of the three-dimensional climatological velocity field are not available due to the sparsity of direct ocean current measurements. So, in this study we rely on the hydrographic observations for adjusting the ocean circulation pattern. Figure 2 gives the optimal current velocity fields at the surface and at the depth of 2400 m for February and August. The surface fields display a clear two-gyre circulation system: the subtropical gyre with the associated Gulf Stream and the subpolar gyre with the Labrador Current. The seasonal signal is distinct as both gyres are strengthened in wintertime in direct response to the intensified westerlies. At the deeper levels, shown by the fields at the depth of 2400 m, an intense deep western boundary current (DWBC) originates from the East Greenland continental slope near the model's northern boundary and flows all the way southward to the model's southern boundary. The DWBC seems to be stronger in summer than in winter.

The North Atlantic meridional circulation, which features a net northward flow in the upper ocean and a net southward flow in the deep ocean, can be viewed clearly in the plot of the zonally averaged meridional mass transport (Figs. 3a,b). The three well-known overturning cells are readily identified: 1) the shallow wind-induced Ekman cell in the surface layer with a maximum of $\sim$7 Sv in wintertime, and 2) the NADW cell, which dominates the whole picture and reaches a maximum strength of $\sim$19 Sv in summertime. The annual average is $\sim$17 Sv, in good agreement with the recent estimate of Schmitz and McCartney (1993). Finally, 3) the deep Antarctic Bottom Water (AABW) cell is present below 3000 m at the southern end. All three cells exhibit substantial seasonal changes. The surface Ekman cell in the subtropics is at its maximum in February while the NADW cell is more intense and deeper in August. The AABW cell also presents an unexpected strong seasonal variation and is intensified in boreal summertime. The enhanced Ekman sucking in the subpolar region in winter counteracts the deep-water formation process leading to a reduction of NADW, a weaker overturning cell, and the weaker DWBC in winter (Figs. 2b and 2d). On the other hand, the changes in the deep AABW cell are induced by the changes in the Levitus (1994a) salinity data in which the water below 3500 m at 10°N is saltier in summer by 0.035 psu with respect to winter. This forces the summer denser deep water to sink along the southern boundary and therefore the AABW cell is intensified.

The heat transport in February and August is shown in Fig. 3c. Clearly the north Atlantic Ocean gains heat year round. But the magnitude of the transport varies with latitude and season and the variations are large especially in mid and low latitudes. The heat transport in February reaches the maximum value of 0.9 PW at 15°N in wintertime, while its maximum of 0.85 PW is located at 25°N in summertime. Comparison with results of prognostic calculations will be made in the following when comparing the annual means of these seasonal optimizations with the estimates of the steady-state inversions.

b. Temperature and salinity fields

The Levitus (1994a,b) sea surface temperature (SST), the modeled optimal SST, and their difference are shown in Fig. 4 for February and August. The seasonal changes of the SST are marked by the basinwide northward migration of isotherms as waters warm up in summertime. The patterns show that the inversion, while reproducing the overall large-scale SST structure, induces also important differences from the Levitus climatology, such as the noticeable intensification of the Gulf Stream jet. The latter is absent in the climatology largely due to the heavy smoothing and averaging of the data. The

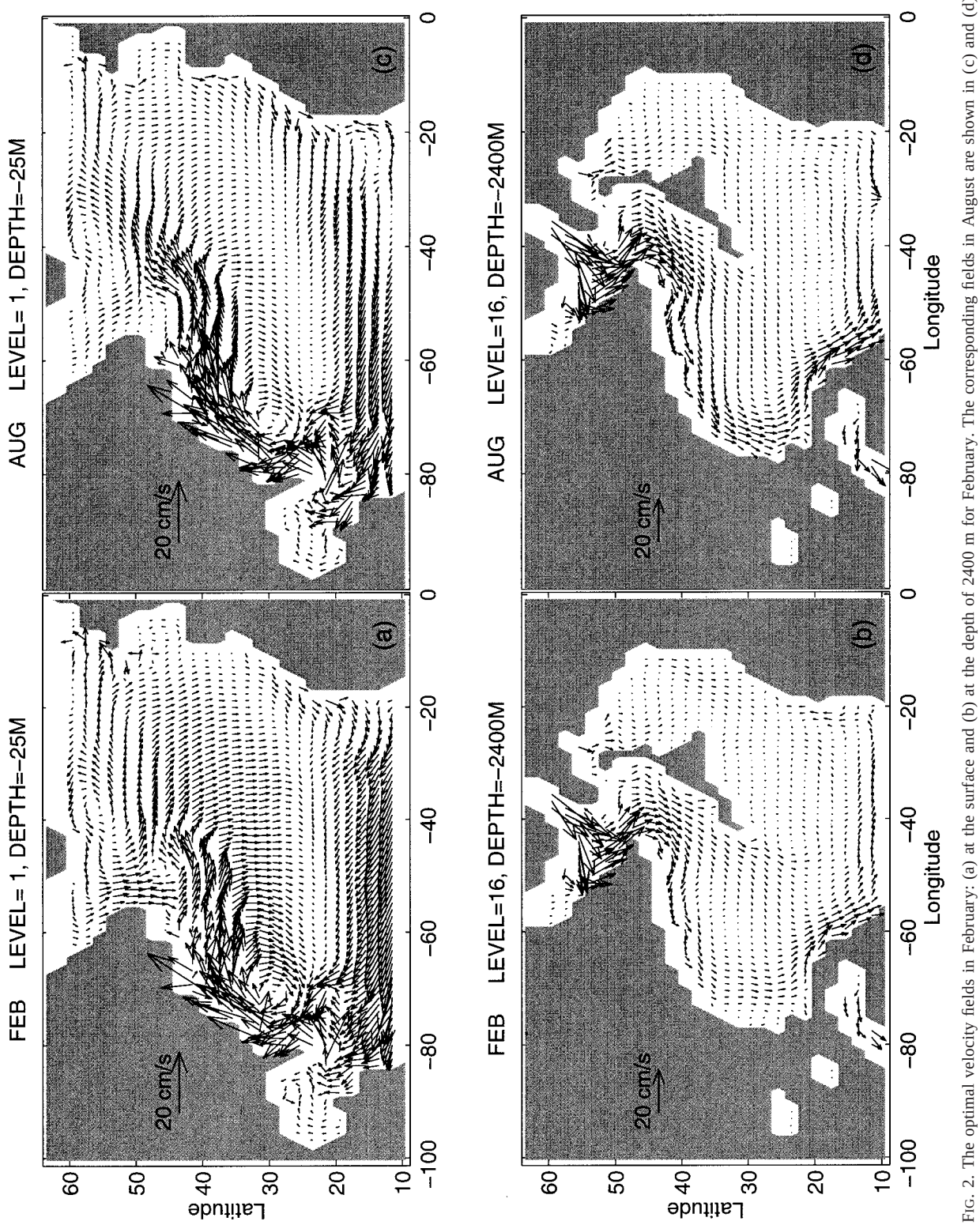

FIG. 2. The optimal velocity fields in February: (a) at the surface and (b) at the depth of 2400 m for February. The corresponding fields in August are shown in (c) and (d).

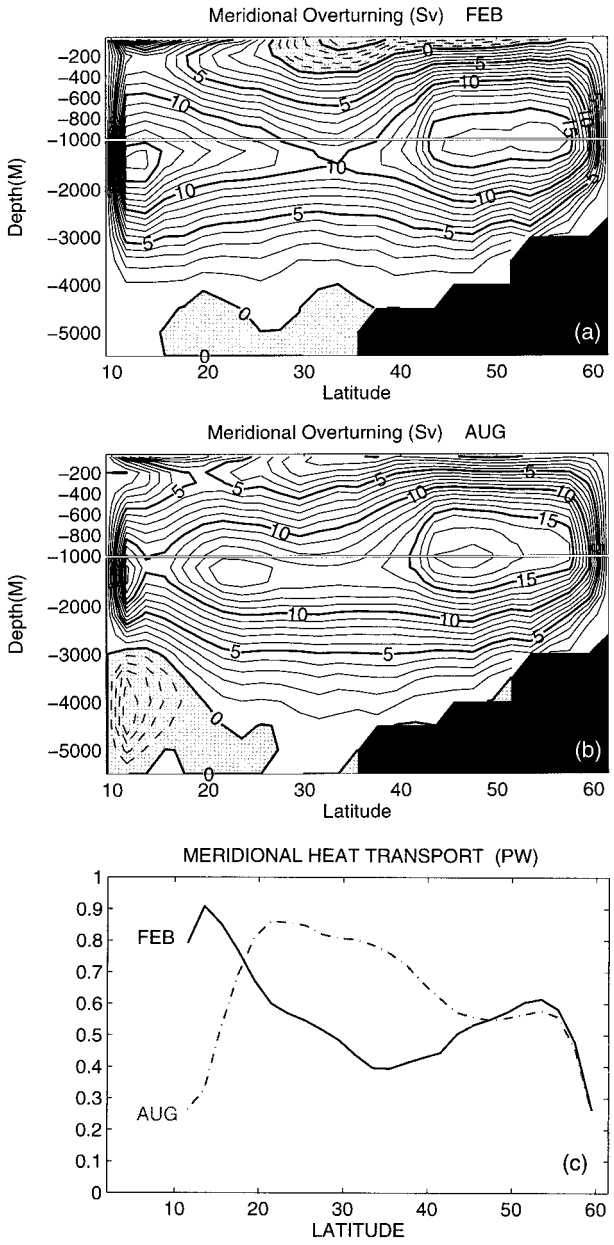

FIG. 3. The zonally averaged meridional transport streamfunction (contour interval is 1 Sv) (a) in February and (b) in August. The total heat transport for February and August is shown in (c).

assimilation recovers the Gulf Stream front thanks to the nonlinear dynamics of the model used. The surface circulation is mainly wind driven and the jet structure is also well reproduced in the modeled velocity field (Fig. 2).

The plots of model–data difference (Figs. 4c and 4f) reveal that the modeled temperature is overestimated with respect to Levitus in the regions associated with the Gulf Stream and is underestimated near the southern boundary. Several factors can contribute to these differences, which include the data, the model, and the boundary conditions. The mismatch between the model and the climatology in the Gulf Stream region is due to the model's correction of the climatology, in which the Gulf Stream front is smeared as shown in Fig. 4a. However, the mismatch appearing north of 40°N results mainly from the separation of the Gulf Stream from the coastline being located too far north. The overshooting of the Gulf Stream to the north is a deficiency common to most prognostic OGCM's calculations (see Semtner and Chervin 1988; Beckmann et al. 1994a,b, among others). It can be seen from the surface velocity fields (Figs. 2a and 2c) that the separation occurs near 40°N, north of Cape Hatteras. This northward overshooting, not corrected by the adjoint, leads to more warm and salty waters transported from the south and gives a large but localized excess of temperature (Fig. 4) and also of salinity (Fig. 5) around 40°–50°N. The excessive warm and salty water lingers in the subpolar region and elevates the temperature and salinity in the area (Figs. 5 and 6).

The underestimated SST near the southern boundary is a boundary-related difference. The exclusion of the tropical ocean shuts off the warm water source and the use of the buffer zone is insufficient to mimic the incoming water transport. This emerges in the model–data difference field at the meridional section along 30°W (Fig. 6). The underrepresentation of the tropical water transport affects the southernmost region and the influence is more pronounced in the upper layer where a mismatch of ~1°C appears. Figure 6 also displays the temperature vertical structure of the subpolar warm and salty anomaly.

Figures 4 and 5 illustrate also that, even though the northern and southern buffer zones may be deficient in mimicking respectively the transports of polar and tropical waters, they do not affect the model interior in the optimization. In fact, in a purely prognostic calculation in which the surface temperature and salinity are relaxed to Levitus everywhere in the domain, the surface fields would just be the Levitus fields given by Figs. 4a,d. The significant differences between the optimized temperatures of Figs. 4b,e and Levitus, clearly evident in the misfits of Figs. 4c,f for temperature and 5a,b for salinity, demonstrate that the buffer zones do not constrain the overall optimization.

c. Surface heat and freshwater fluxes

The surface monthly heat and freshwater ($E - P$) fluxes are determined by the optimization procedure. The patterns in February and August (Fig. 7) indicate that the seasonal variance is large. The whole basin switches from releasing heat almost everywhere in February to receiving heat in August. The change is particularly dramatic in the warm core of the Gulf Stream, its heat loss (>400 W m^{-2}) in winter being much larger than its heat gain (<100 W m^{-2}) in sum-

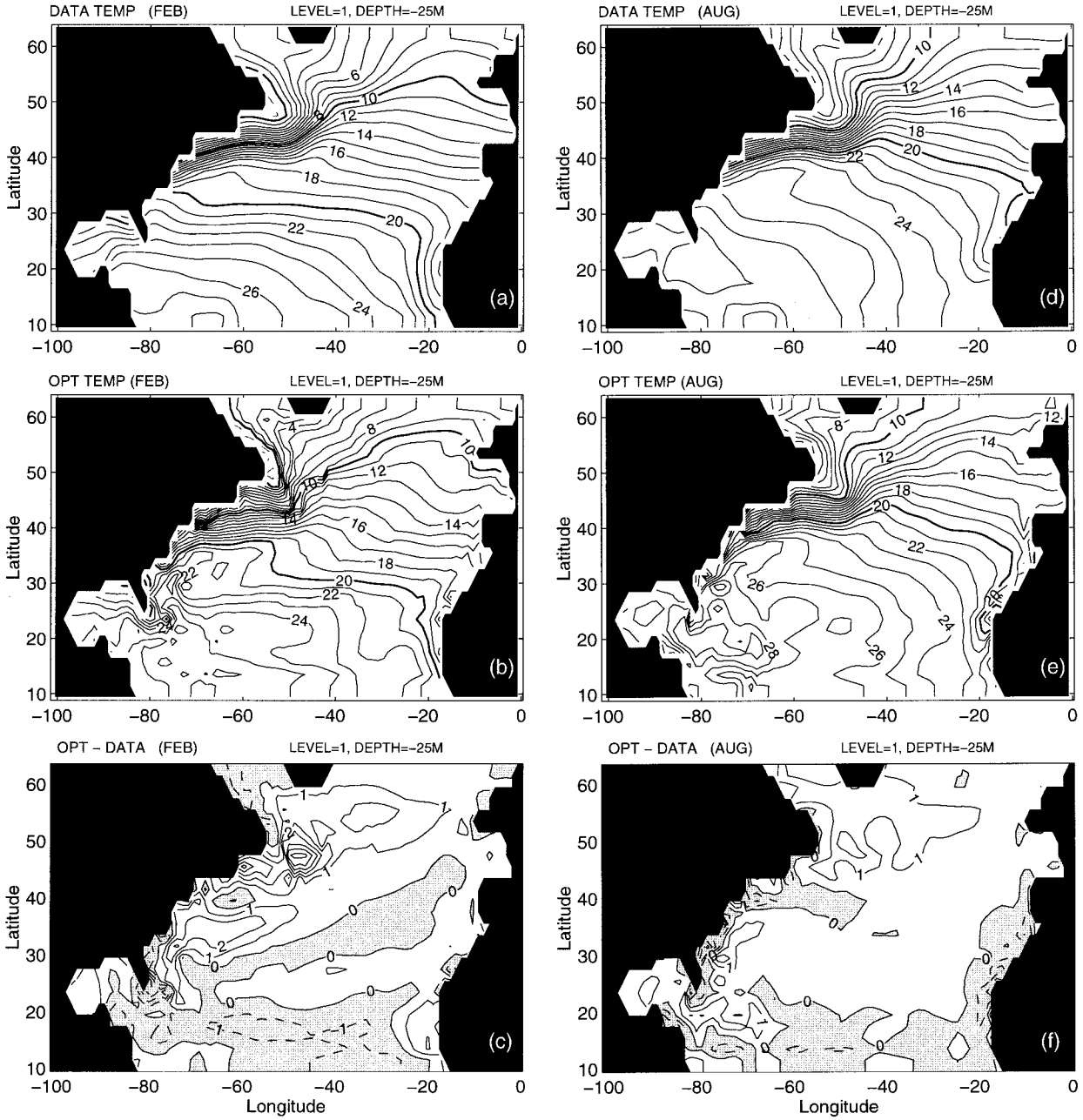

FIG. 4. The surface temperature fields in February: (a) the SST from the Levitus (1994b) climatology; (b) the optimal SST from the seasonal assimilation; (c) the difference between the optimal SST and the climatological SST. The corresponding SST patterns and their difference in August are shown in (d), (e), and (f). Contour interval is 1°C for all plots.

mer. In winter the decreased solar radiation, the large air–sea temperature difference, the large dewpoint–sea temperature difference, and the intensified westerlies all contribute to the strong ocean heat release. The adjoint calculation, which infers the fluxes directly from the hydrographic information, reproduces well the dominating features of the seasonal heat flux variations.

The freshwater flux in February displays two major $E - P$ (>200 cm yr^{-1}) maxima, one is associated with the waters of the Gulf Stream and the other lies near the model's southern boundary. In August the former becomes less than zero (i.e., a net precipitation) and the latter moves its center eastward. The seasonal changes in the eastern midlatitudes are small, with evaporation prevailing over precipitation year round with a magnitude of 50–100 cm yr^{-1}. The changes in the region of the subpolar gyre are evident. The net precipitation center intensifies and stretches southward in wintertime.

As is stated in section 2c, the adjoint procedure takes

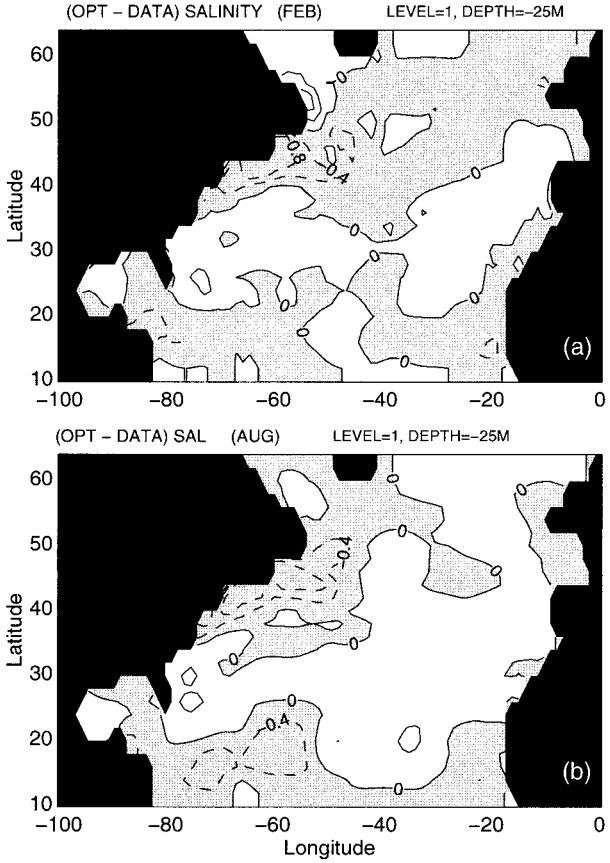

FIG. 5. The model–data difference for the surface salinity field (a) in February and (b) in August (contour interval is 0.4 psu).

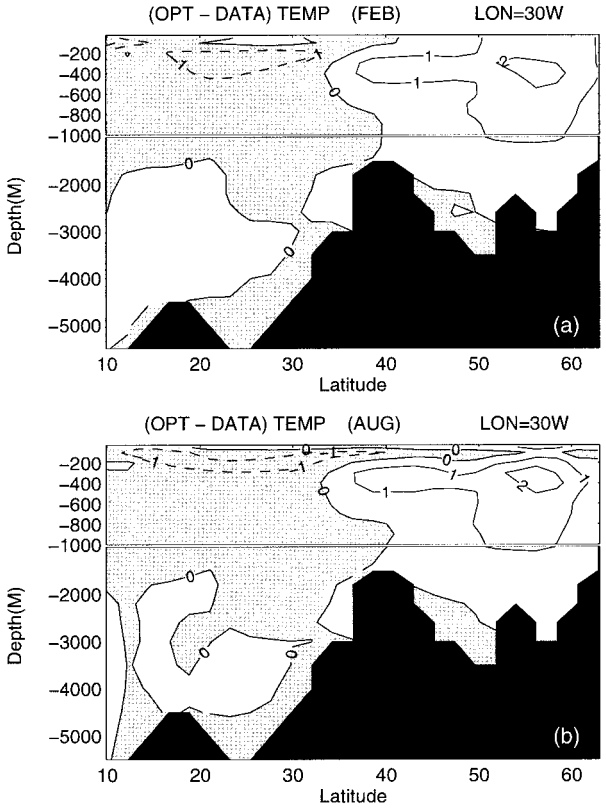

FIG. 6. The model–data difference along the meridional section at 30°W in (a) February and (b) August (contour interval is 1°C).

the Oberhuber (1988) fluxes as the first guess and makes the adjustment iteratively based on the model dynamics and the hydrographic data information. The adjustment is, however, not constrained directly by the climatological fluxes since the cost function does not include the flux penalty. To delineate the adjustments brought by the adjoint assimilation, we provide the Oberhuber fluxes in Fig. 8 as a reference. These fluxes however should not be used to verify the adjoint calculations since they themselves contain large uncertainties as many studies have indicated (e.g., Schiller 1995).

The gross seasonal variation of the estimated surface heat flux is similar to that of the Oberhuber heat flux, as both display the seasonal reversal of the air–sea heat exchange. A detailed comparison of these two maps shows that the magnitude of the estimated heat release in winter is relatively larger than that of the climatology. The patterns of the optimal SST and its model–data difference (Fig. 4) may cast some light on the reason for this adjustment. The intensified heat release in the region of the Gulf Stream and its recirculation reflects the model's tendency to intensify the smeared Gulf Stream front of the Levitus climatology. Establishing the model-favored Gulf Stream front requires the transport of warm waters from the south, but this warm water pool is regarded as an anomaly due to the data constraint. Therefore the ocean needs to release additional heat to the atmosphere to stay closer to the data. The larger heat release in the subpolar region is also induced by the warm water anomaly. The comparison further shows that the estimation is blended with some small-scale heat transfers especially along the model's western boundary. These noiselike features may be induced by the Levitus climatology in which the data are averaged isobarically and anomalous water masses may be therefore produced (Lozier et al. 1994).

The estimation of the freshwater flux exhibits similar traits to that of the heat flux: the magnitude is intensified and the pattern is less smooth. In addition, the estimation clearly shows the northward shift of the modeled Gulf Stream. The freshwater gain in that region is required to suppress the salty water excesses. The estimated pattern also reveals that the $E - P$ maximum in the subtropics near the southern boundary moves eastward in summertime, consistent with the climatology of Schmitt et al. (1989) but different from the Oberhuber climatology.

5. The mean state averaged over the seasonal cycle versus the steady state

In this section, we average the results over one full seasonal cycle and compare quantitatively the resulting

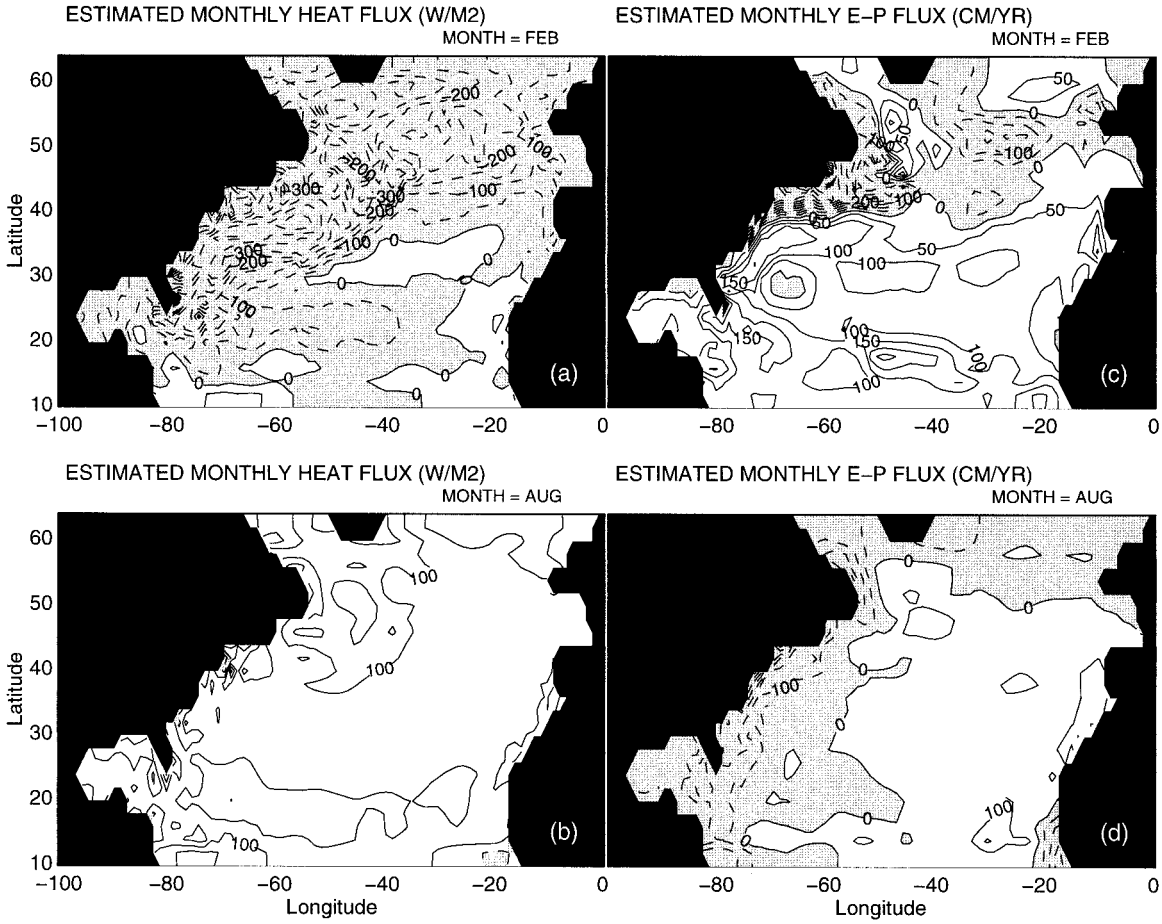

FIG. 7. The optimally determined surface heat flux for (a) February and (b) August (contour interval is 50 W m^{-2}). The optimal surface freshwater flux ($E - P$) for (c) February and (d) August (contour interval is 50 cm yr^{-1}).

annually averaged mean state with the *steady state* obtained from the steady calculations of YM96. In the steady case, the forcings are assumed to be time invariant. The annual mean Hellerman and Rosenstein wind stress is applied, and steady heat and freshwater fluxes are determined from assimilating the annual mean Levitus climatology (see YM96 for details). Quantitative comparisons with results of the prognostic calculations of Holland and Bryan (1994) are also made whenever meaningful.

a. Barotropic transport

The barotropic transport streamfunction, representing the vertically averaged flow field, is shown in Fig. 9. The barotropic transports computed from the two calculations are quite similar in the overall pattern, but in the region of the Gulf Stream extension the seasonal forcings produce more northeastward transport due to the intensified Gulf Stream that pushes the subpolar gyre northward. The maximum intensity of the western boundary transport for the seasonal run reaches ~41 Sv, 2 Sv stronger than that of the steady run. Both values are comparable to that of prognostic simulations of Holland and Bryan (1994). Consistent with the barotropic transport streamfunction, the two current velocity fields (not shown) have a great similarity in both magnitude and structure.

b. Meridional circulation and poleward heat transport

A comparison of the zonally averaged meridional transports (Fig. 10) reveals that the differences between the two overturning cells are small. The mean state averaged over the seasonal cycle clearly smoothes out the strong seasonal variability shown in Fig. 3, resulting in a surface Ekman cell and a AABW cell with magnitudes similar to those of the steady case. In both cases, the intensity of the NADW cell of ~17 Sv is quite realistic (Schmitz and McCartney 1993) and comparable to the values of coarse-resolution prognostic calculations (Böning et al. 1995). However, the seasonal forcings produce some differences: a boundary-related cell exists at the depth of 1000 m adjacent to the model's southern boundary in the annually averaged mean state. This fea-

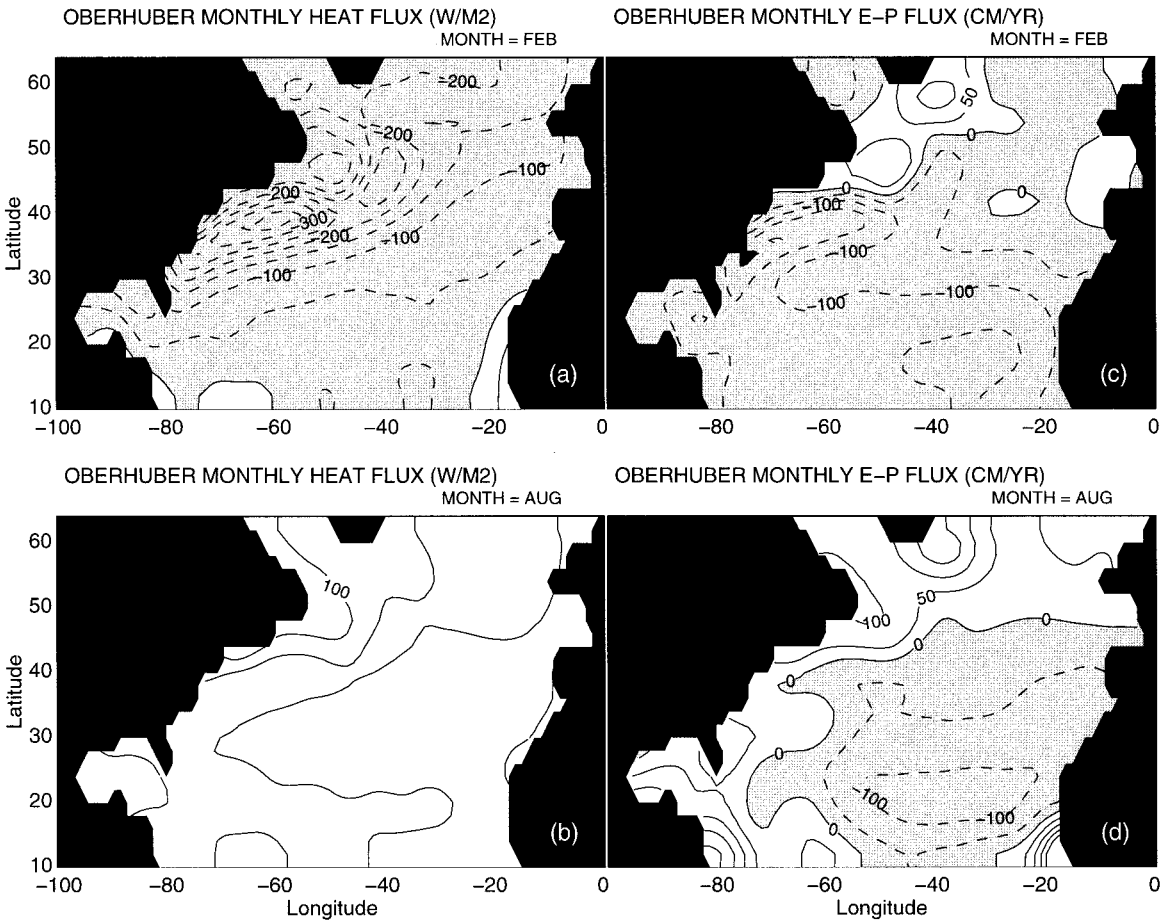

FIG. 8. The Oberhuber climatological surface fluxes: heat flux in (a) February and (b) August (contour interval is 50 W m^{-2}), and freshwater flux in (c) February and (d) August (contour interval is 50 cm yr^{-1}).

ture persists year round and changes slightly with seasons (Fig. 3).

Despite the great similarity in the mean three-dimensional circulations between the two experiments, there is a large difference in the magnitude of the two total poleward heat transports (Fig. 10c). The heat transport is enhanced over the whole region when the seasonal cycle is included, and the improvement is most significant at lower latitudes where an increase of more than 0.2 PW is found. On the other hand, the latitudinal distributions of the two heat transports are quite similar, both have a higher northward heat transport at low and midlatitudes. Figure 10c also shows the heat transport in February and August. One can observe that the large seasonal variation in the mid and low latitudes is canceled out in the annual average. The averaged mean transport has a value of 0.7 PW at 25°N, which is smaller than the estimate from Hall and Bryden (1982). Nevertheless, the improvement produced by the seasonal forcings over the steady-state estimates is quite significant and comparable to the heat transports of the prognostic calculations (Holland and Bryan 1994), equally underestimated. We believe that the underestimation of the poleward heat transport, in spite of the realistic strength of the NADW cell, is due to the use of the traditional horizontal eddy diffusivity coefficient, as pointed out by Böning et al. (1995) and discussed in the introduction.

The large increase in the total poleward heat transport in the seasonal assimilation shows the important role played by the seasonal forcings. We now examine the dynamical mechanisms responsible for this change. Note that the total poleward heat transport constitutes the heat transports due to advection and due to diffusion. However the contribution from the diffusion field is near zero both in this experiment and in the previous steady experiment and is therefore excluded in the following discussion.

In the presence of the seasonal forcing, the temperature and the meridional component of the velocity can be written as

$$T = \overline{T} + T' \quad \text{and} \quad v = \overline{v} + v', \tag{16}$$

where the quantities with an overbar represent the time-mean state averaged over the seasonal cycle and the quantities with a prime are the seasonal anomaly from

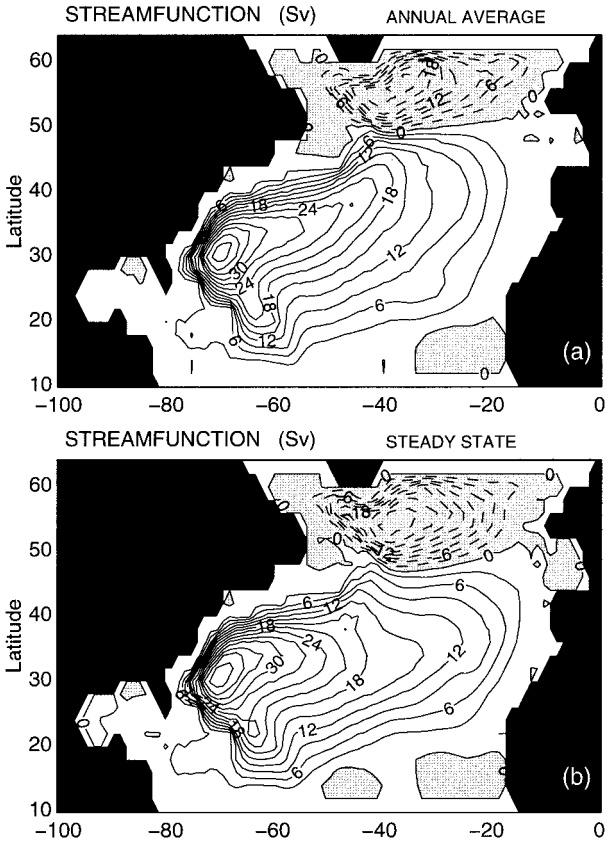

FIG. 9. The mean state of the vertically integrated barotropical transport streamfunction (Sv) obtained from (a) the average over the seasonal cycle and (b) the previous steady-state assimilation (contour interval is 3 Sv).

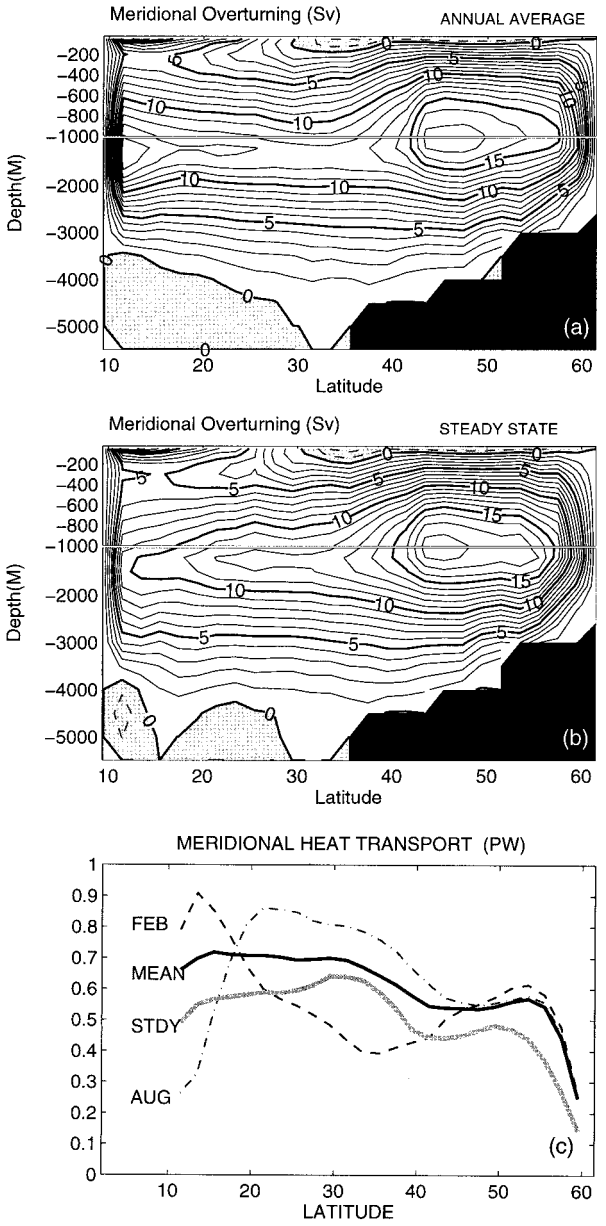

FIG. 10. The mean state of the zonally averaged meridional transport streamfunction obtained from (a) the average over the seasonal cycle and (b) the previous steady-state assimilation (contour interval is 1 Sv). The total heat transport is shown in (c) for the annual average (MEAN), the steady state (STDY), February (FEB), and August (AUG).

the annual averaged state. Since the model is in a steady seasonal state, we have

$$\overline{T'} = 0 \quad \text{and} \quad \overline{v'} = 0. \tag{17}$$

Then the poleward heat transport due to advection, if averaged over one seasonal cycle, is

$$\mathrm{HT}_{\mathrm{average}} \equiv \rho c_p[\overline{vT}] = \underbrace{\rho c_p[\overline{v}][\overline{T}]}_{\mathrm{HT}_{\mathrm{A1}}} + \underbrace{\rho c_p[\overline{v'T'}]}_{\mathrm{HT}_{\mathrm{A2}}}, \tag{18}$$

where the square brackets denote the longitudinal and depth averages. Here $\mathrm{HT}_{\mathrm{A1}}$ is the contribution from the mean temperature and velocity fields, while $\mathrm{HT}_{\mathrm{A2}}$ is the contribution from the seasonal anomaly fields.

On the other hand, the poleward advective heat transport obtained from the steady assimilation of YM96 is

$$\mathrm{HT}_{\mathrm{steady}} = \rho c_p[v]_{\mathrm{steady}}[T]_{\mathrm{steady}}, \tag{19}$$

where $[v]_{\mathrm{steady}}$ and $[T]_{\mathrm{steady}}$ are the longitudinal and depth-averaged quantities of the steady field.

The analysis shows that, though $\mathrm{HT}_{\mathrm{A2}}$ is an order smaller than $\mathrm{HT}_{\mathrm{A1}}$, its value is positive at all latitudes except at the very few southern and the northern boundary points. This indicates that the heat transport made by the seasonally anomalous fields has an overall positive effect and is not negligible. Its influence on the total heat transport, as well as on the temperature fields, is illustrated by the diagram in Fig. 11. The positive $\mathrm{HT}_{\mathrm{A2}}$ makes two contributions, the first is to increase $\mathrm{HT}_{\mathrm{average}}$ directly by the relation (18) and the second to warm up the ocean. The effect of the latter mechanism is mostly reflected in the surface water. As a consequence, the mean field alone ($\mathrm{HT}_{\mathrm{A1}}$) transports more heat northward than the steady field $\mathrm{HT}_{\mathrm{steady}}$.

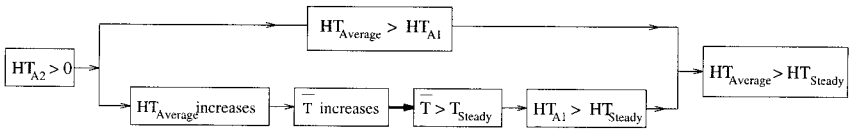

FIG. 11. The contribution of a positive transport by the seasonal anomaly fields to the improvement of the total heat transport. The positive HT_{A2} increases the total heat transport and warms up the water in particular at the upper layer.

c. Temperature and salinity fields

A comparison of the mean SSTs from the climatology, the average over the seasonal cycle, and the steady state (Figs. 12a–c) shows that the seasonal forcings induce a remarkable improvement in the SST simulation. In contrast to the steady case, the modeled annually averaged SST not only is much smoother, but has a better large-scale structure and a much better Gulf Stream Front. The model–data misfits (Figs. 12d and 12e) further confirm that the contrast between the experiments with or without the seasonal cycle is striking. The peculiar intensive surface cooling in the steady case essentially disappears when including the seasonal cycle. The annually averaged SST misfit field shows that the fit between the model and the climatology is, in general, satisfactory as the differences are largely within the prespecified error estimate except at a few places near the model's western boundary. These few exceptions, as the analysis of section 4b indicates, are the results of the biased representation of the ocean state either by the climatology or by the model at these places.

The elimination of the basin-scale surface cooling in the seasonal assimilation confirms that the cause of this bias is indeed the lack of the seasonal cycle. YM96 have found that, in the absence of the seasonal cycle, the modeled steady state produces a warm deep ocean compensated by a cool surface water. The reason, deduced by YM96, is that the deep water in the present model configuration is formed through an artificial sinking of the surface water within the imposed buffer zone. Since the annual mean surface water is warmer than the winter surface water, the modeled surface water, which is the source for the deep water, has to be made cooler in order to reduce the large data misfits in the deep ocean. It follows that assimilating the winter climatology might be enough for the rectification. However, the experiment driven by the winter wind stress and constrained to the Levitus winter climatology, although it reduced the magnitude of the surface cooling, does not solve the problem (unpublished results). This indicates that using the winter climatology is only a partial remedy for the surface cooling. The results from the seasonal assimilation demonstrate that other mechanisms operate when the seasonal cycle is included. The mechanism identified in this study is the heat transport contributed from the temperature and velocity seasonal anomaly fields, denoted by HT_{A2} in (18), as discussed in the previous subsection.

The better fit between model and data temperature fields in the seasonal assimilation can also be observed in the meridional section along 30°W (Figs. 13a–c). Examination of Figs. 13d,e shows the effects of the seasonal forcings in shutting down the large surface cooling and in reducing the magnitude of the model–data misfits as discussed above. The simulation of the salinity fields, on the other hand, seems to be less affected by the seasonal forcing (Figs. 14a–c). There are no major overall differences in either the pattern or the magnitude between the experiments with and without the seasonal cycle, but the isohalines are rather bumpy in the steady case. The plots of the model–data misfits (Figs. 14d,e) indicate that the mismatches over almost the entire basin are below the prespecified standard deviation except in the region associated with the Gulf Stream separation. The weak dependence of the salinity simulation on the seasonal forcings reflects that the atmospheric feedbacks to the salinity field are not critical, although its absence in the heat flux formulation results in a large SST drift (Sirkes and Tziperman 1995). In addition, it indicates that the adjustment of the haline structure occurs on a much longer timescale.

d. Surface heat and freshwater fluxes

Apart from improving the simulation of the temperature field and the poleward heat transport, the seasonal forcing also induces a dramatic improvement in the estimation of the annual surface heat and freshwater fluxes (Fig. 15). The mean surface fluxes averaged over the seasonal cycle resemble more closely the patterns from the Oberhuber climatology, and the strong seasonal variations shown in Fig. 7 are largely smoothed out. But the signature of the northward shifting of the Gulf Stream separation is still shown in the annually averaged freshwater flux.

On the other hand, the surface fluxes estimated from the steady forcings are (Figs. 15b and 15e) far from the climatology. They are also not comparable with the annually averaged mean fluxes from the seasonal assimilation. The magnitude of the steady fluxes is much larger and the patterns are poorly contaminated by many localized intensive heat/salt adjustments. The problem is especially severe for the freshwater flux estimation. Noisy flux estimations resulting from assimilating the annual mean Levitus climatology under the steady-state assumption have been reported in previous studies (Tziperman et al. 1992; Schiller 1995; YM96). It has been suggested that the data quality in the Levitus (1982) cli-

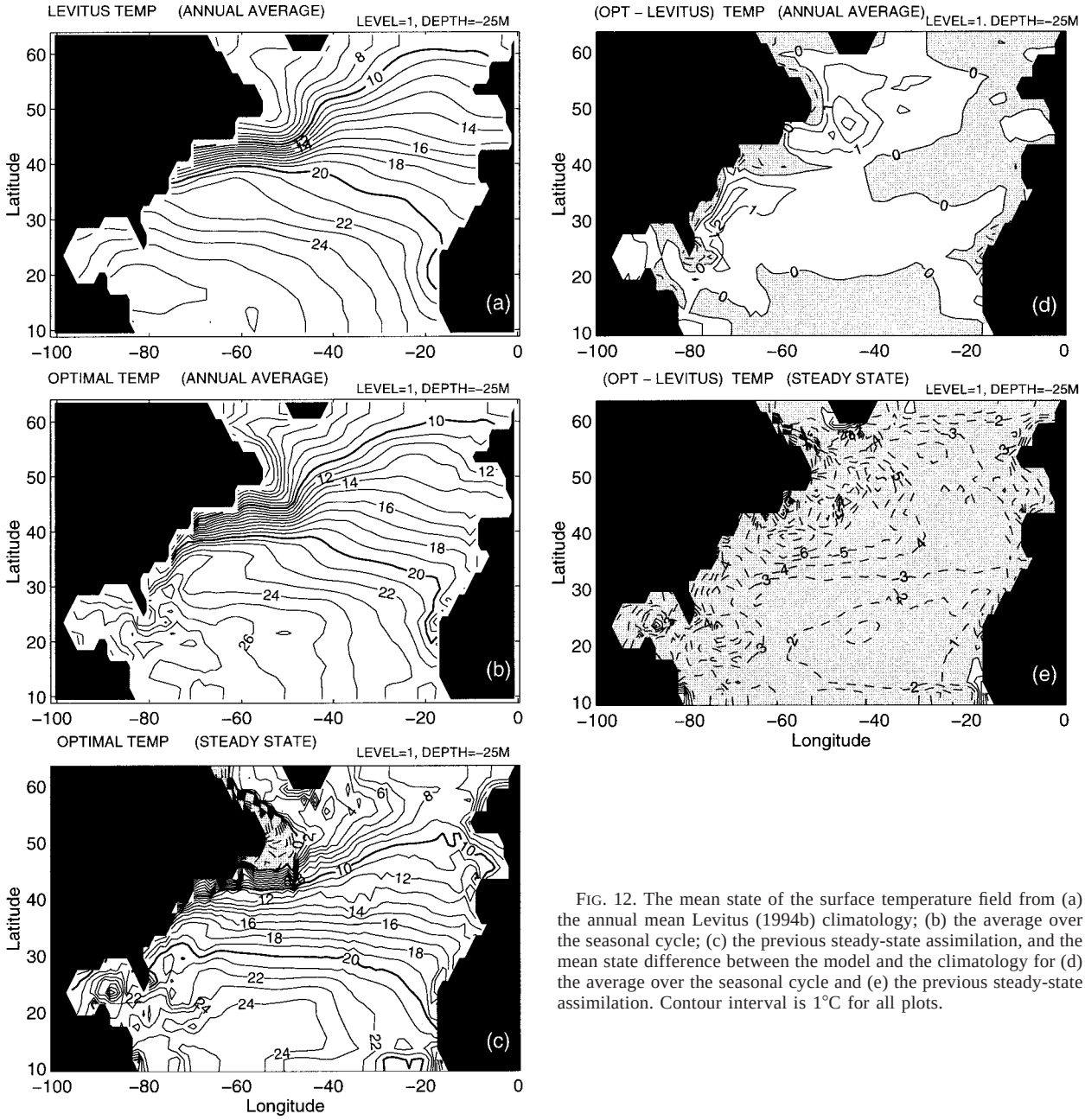

FIG. 12. The mean state of the surface temperature field from (a) the annual mean Levitus (1994b) climatology; (b) the average over the seasonal cycle; (c) the previous steady-state assimilation, and the mean state difference between the model and the climatology for (d) the average over the seasonal cycle and (e) the previous steady-state assimilation. Contour interval is 1°C for all plots.

matology may be the cause of the problem. Indeed, when using the Levitus (1994a,b) new climatology, steady optimizations give flux estimates better than those obtained from using the Levitus (1982) old climatology (unpublished results). But the noise prevailing over higher latitudes still does not vanish. The dramatic changes brought by the seasonal forcings demonstrate that, in addition to data quality, the dynamics and the added degree of freedom in the parameter estimation play crucial roles. The seasonal forcings eliminate the surface cooling and give a seasonal modulation, which in turn leads to an improved representation of the upper ocean demanding less from the surface fluxes for fitting the model to the data. On the other hand, although estimating the monthly flux patterns introduces more control parameters and requires more computational time, the system is given more degree of freedom in the parameter adjustment, which also contributes to a smoother estimation.

6. Summary and conclusions

The study presents an adjoint OGCM assimilation of the North Atlantic circulation and hydrography with the seasonal cycle included, representing a significant step

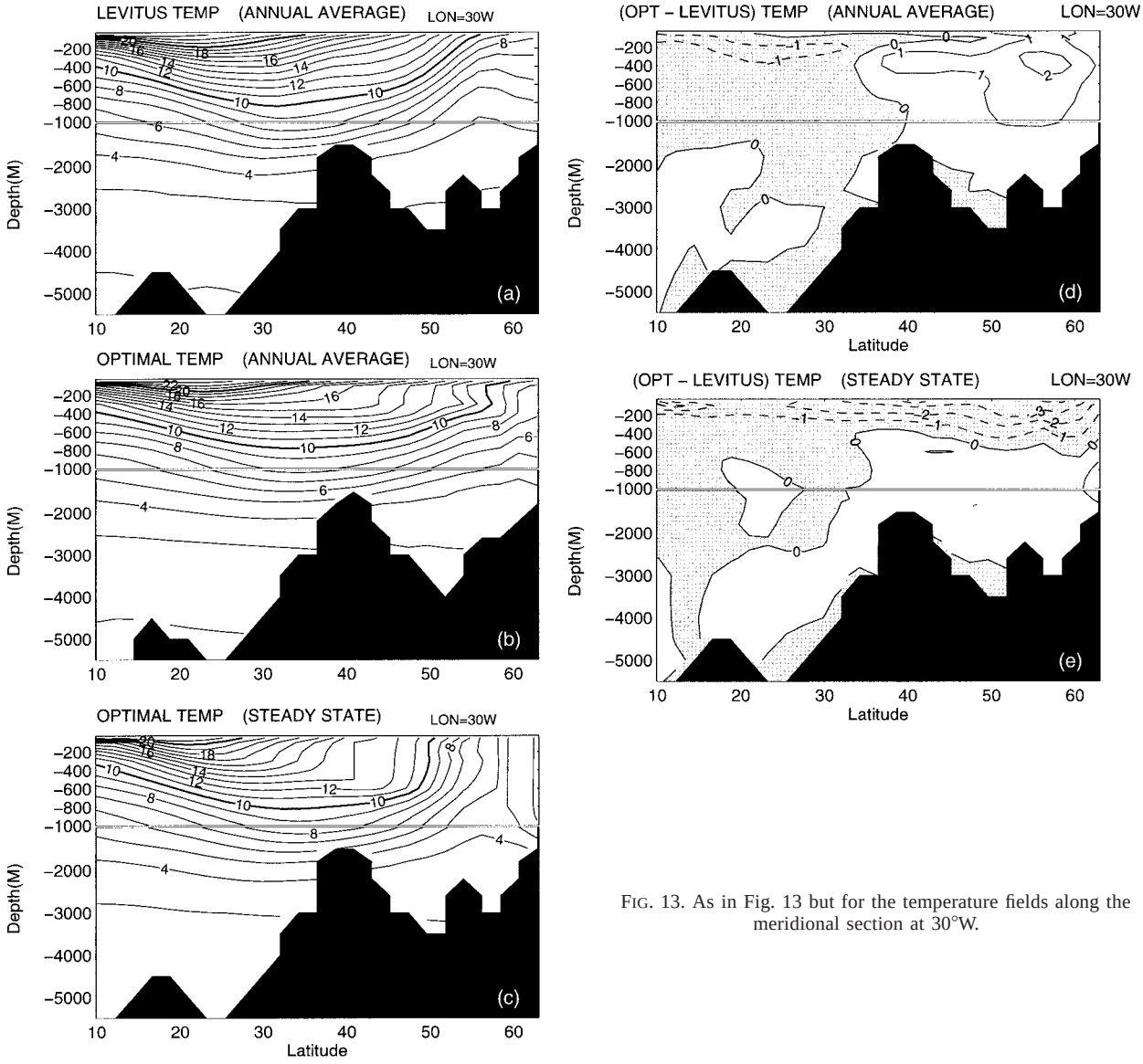

FIG. 13. As in Fig. 13 but for the temperature fields along the meridional section at 30°W.

forward over the previous assimilations with the steady-state assumption. The model's initial conditions and the monthly surface heat and freshwater fluxes are optimally estimated in search of an ocean state consistent with the Levitus (1994a,b) monthly climatology. The primary goal of the study is to estimate large-scale oceanic properties important for climate issues and how these optimized estimates are improved by the inclusion of the seasonal cycle in the adjoint assimilation.

The inversion shows that the North Atlantic ocean circulation exhibits strong seasonal variations as expected. Both subtropical and subpolar gyres are strengthened in wintertime as a direct result of the westerly intensification. The zonally integrated meridional mass transport displays that the NADW cell is weaker in winter and stronger in summer, which is opposite to the changes in the surface Ekman cell. The seasonal changes in the total poleward heat transport is also evident. Although the heat transport is northward year round over the whole model domain, its amplitude changes greatly with seasons. The wind forcing is the controlling factor for all these seasonal changes.

The seasonal variations of the North Atlantic climatological hydrography are well reproduced by the adjoint inversion. More importantly, the study shows that the assimilation is able to correct the jet structure of the Gulf Stream being smeared in the Levitus (1994b) climatology, thanks to the model nonlinear dynamics in use. The two aspects of the adjoint assimilation are clearly presented: the assimilation not only is able to derive the poorly known parameters (such as the model initial conditions and the upper thermal and haline con-

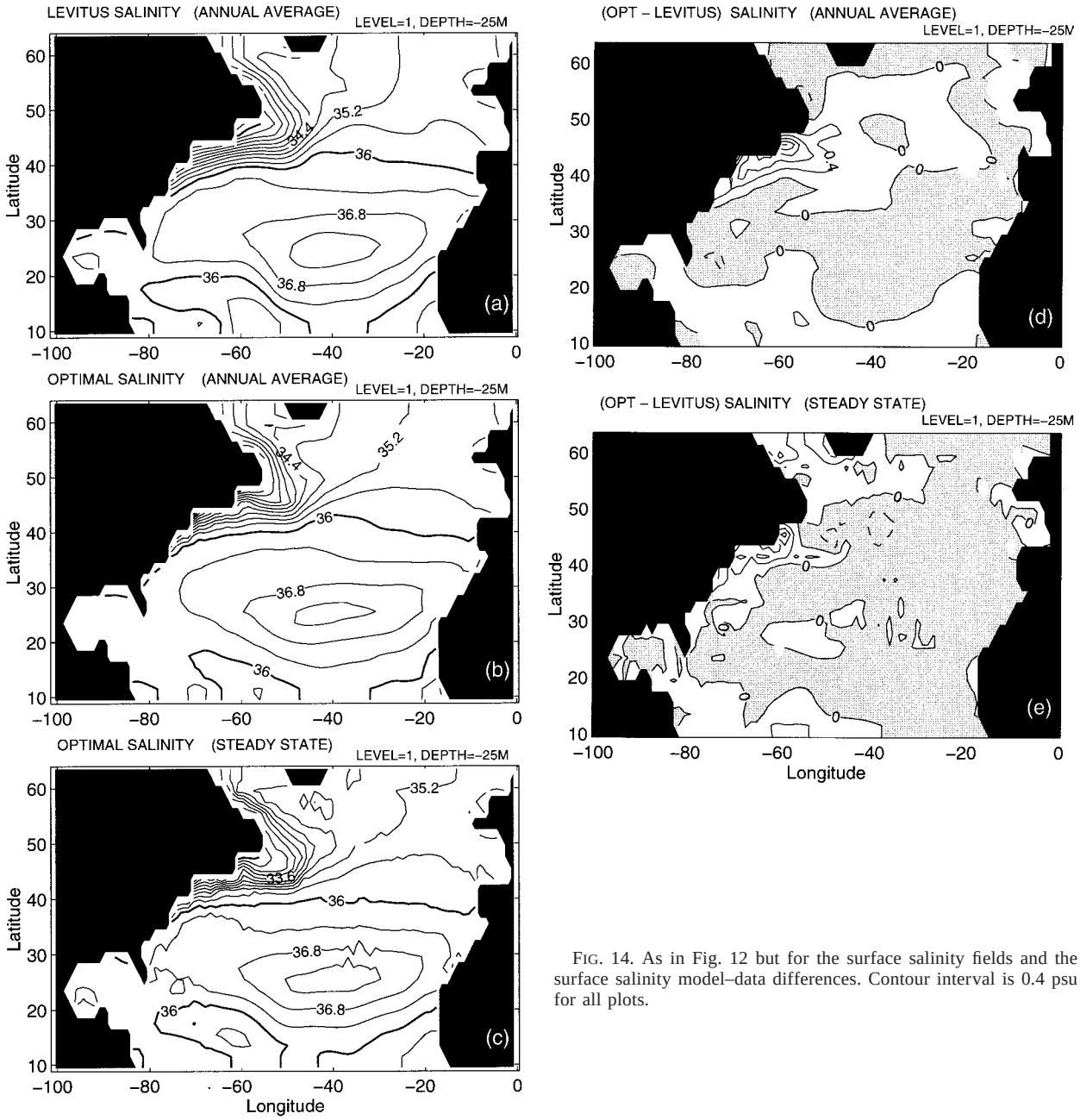

FIG. 14. As in Fig. 12 but for the surface salinity fields and the surface salinity model–data differences. Contour interval is 0.4 psu for all plots.

ditions) but also can make corrections of data information based on the model dynamics. The comparison of the model–data misfits reveals two major misfit areas: the region associated with the Gulf Stream and the subpolar region. The model's northward shift of the Gulf Stream separation, a common deficiency also of prognostic OGCMs, leads to the large but localized excess of temperature and also of salinity in the area.

The comparison between the *mean state* from averaging the monthly calculations over the seasonal cycle and the *steady state* from the previous steady assimilation of YM96 reveals that the difference between these two states is significant. Including the seasonal forcings remarkably improves the simulation of the temperature distribution, the estimate of the annual mean total poleward heat transport as well as the estimation of the surface fluxes. The improvements are represented by (i) the basinwide upper-layer cooling with respect to the steady inversion disappears as well as the deep-layer warming; (ii) the poleward heat transport is increased by ~0.2 PW over the whole latitudinal extension; and (iii) the mean optimal surface fluxes averaged over the seasonal cycle resemble closely the patterns from the Oberhuber (1988) climatology, a striking contrast to the

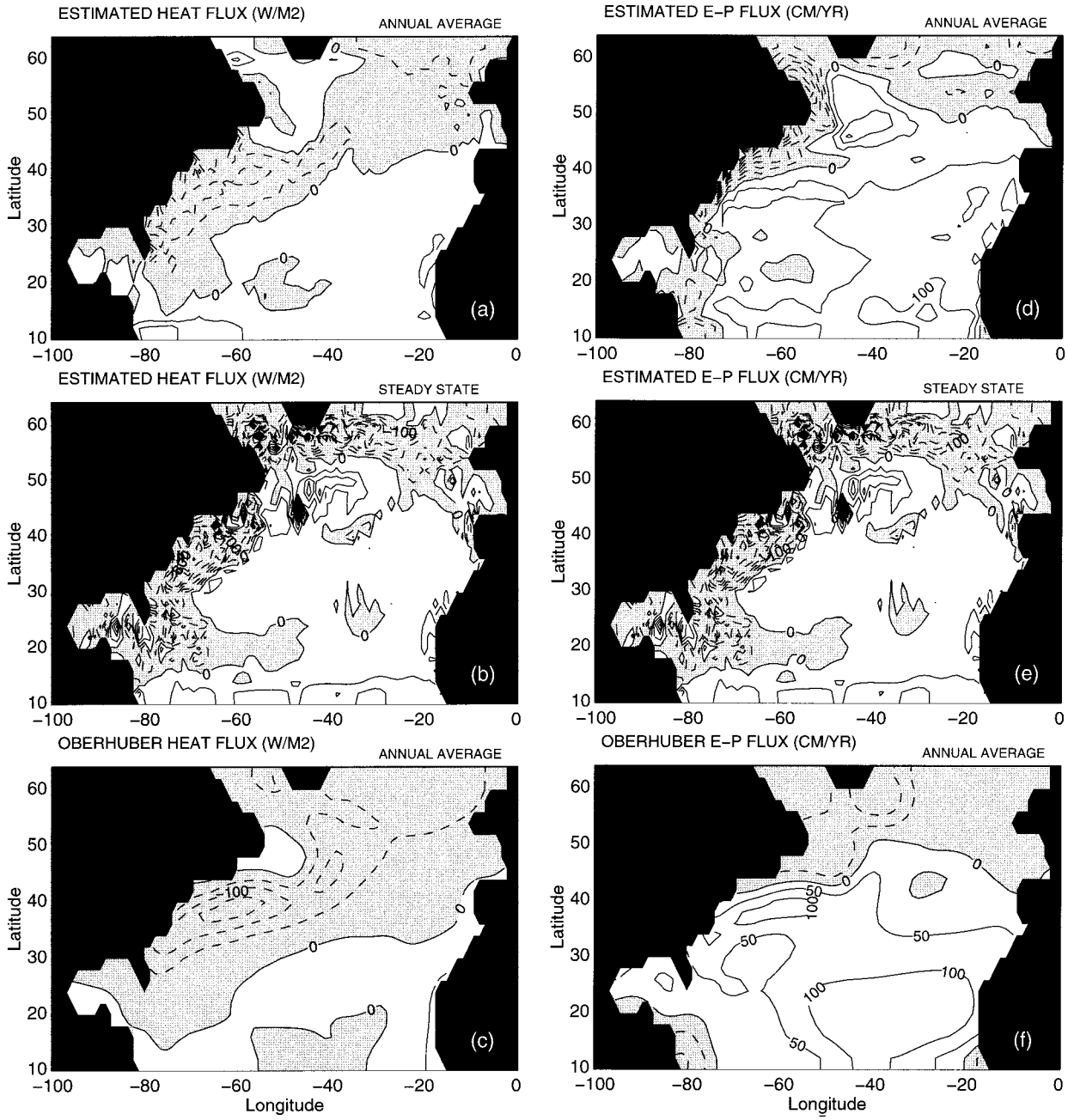

FIG. 15. The mean state of the surface fluxes. Heat flux from (a) the average of the optimally determined monthly fluxes over the seasonal cycle; (b) the previous steady-state assimilation; and (c) the annual mean Oberhuber climatology (contour interval is 50 W m^{-2}). The respective freshwater fluxes ($E - P$) are given in (d), (e), and (f) (contour interval is 50 cm yr^{-1}).

noisy and largely intensified flux estimates from the steady assimilation. However, the impact of seasonal forcings on the three-dimensional circulation is less important. Its impact on the salinity field is also small and there is no drift in the surface salinity in contrast to the temperature. This is expected because the surface haline flux condition does not depend on the atmospheric feedbacks, although its absence in the heat flux formulation can result in the large surface temperature drifting according to Sirkes and Tziperman (1995).

The analysis shows that the heat transport made by the seasonally anomalous fields, $\overline{[v'T']}$, plays an important role. This term is missing in experiments with steady forcings. Although $\overline{[v'T']}$ is an order of magnitude smaller than that of the transport made by the annual mean fields, $\overline{[v]}\,\overline{[T]}$, its value is positive over

the whole model domain. This second-order term has two direct effects: it increases both the total mean heat transport and the overall upper-layer temperatures. The elimination of the surface cooling of the steady simulation results from the combined efforts of the extra heat transport by $\overline{[v'T']}$ and the winter climatology. The winter climatology provides cooler source waters favorable for deep-water formation and has been identified in the study of YM96. However, it is worth noting that the winter climatology alone is not able to terminate the surface cooling. The heat transport by the seasonal anomaly fields $\overline{[v'T']}$ proves to be the most effective rectification means.

The improvement made in the surface flux estimation in the seasonal assimilation is attributable to three factors. Better quality of the Levitus (1994a,b) new climatology reduces the level of data bias and correspondingly reduces the degree of unphysical adjustments. Further, the use of the seasonal forcings provides a reasonable dynamical framework, which not only alleviates the cross-pycnal averaging in the data but also enables the seasonal modulation of the upper ocean during the assimilation. Lastly, estimating the monthly flux patterns, though increasing the number of control parameters, gives the system more degrees of freedom in the adjustment, which contributes to a smoother estimation.

Acknowledgments. The computations were conducted on the Cray-J932 at the NASA/Goddard Space Flight Center. This research was carried out with the support of the National Aeronautics and Space Administration, Grant NAGW-2711 and NAG5-4655. Eli Tziperman is sincerely thanked for his insightful and constructive comments.

REFERENCES

Beckmann, A., C. W. Böning, C. Köberle, and J. Willebrand, 1994a: Effects of increased horizontal resolution in a simulation of the North Atlantic Ocean. *J. Phys. Oceanogr.,* **24,** 326–344.

——, ——, B. Brügge, and D. Stammer, 1994b: On the generation and role of eddy variability in the central North Atlantic Ocean. *J. Geophys. Res.,* **99,** 20 381–20 391.

Bergamasco, A., P. Malanotte-Rizzoli, W. C. Thacker, and R. B. Long, 1993: The seasonal steady circulation of the Eastern Mediterranean determined with the adjoint method. *Deep-Sea Res. II,* **40,** 1269–1294.

Böning, C. W., and P. Herrmann, 1994: Annual cycle of poleward heat transport in the ocean: Results from high-resolution modeling of the North and equatorial Atlantic. *J. Phys. Oceanogr.,* **24,** 91–107.

——, R. Döscher, and R. G. Budich, 1991: Seasonal transport variation in the western subtropical North Atlantic: Experiments with an eddy-resolving model. *J. Phys. Oceanogr.,* **21,** 1271–1289.

——, W. R. Holland, F. O. Bryan, G. Danabasoglu, and J. C. McWilliams, 1995: An overlooked problem in model simulations of the thermohaline circulation and heat transport in the Atlantic Ocean. *J. Climate,* **8,** 515–523.

Bryan, K., 1969: A numerical method for the study of the circulation of the world ocean. *J. Comput. Phys.,* **4,** 347–376.

Cox, M. D., 1984: A primitive equation, three-dimensional model of the ocean. GFDL Ocean Group Tech. Rep. 1, Geophysical Fluid Dynamics Laboratory, 137 pp.

Cummins, P. F., G. Holloway, and A. E. Gargett, 1990: Sensitivity of the GFDL ocean general circulation model to a parameterization of vertical diffusion. *J. Phys. Oceanogr.,* **20,** 817–830.

Daley, R., 1990: *Atmospheric Data Analysis.* Cambridge University Press, 457 pp.

Gent, P. R., and J. C. McWilliams, 1990: Isopycnal mixing in ocean circulation models. *J. Phys. Oceanogr.,* **20,** 150–155.

Ghil, M., and P. Malanotte-Rizzoli, 1991: Data assimilation in meteorology and oceanography. *Advances in Geophysics,* Vol. 33, Academic Press, 141–266.

Hall, M. M., and H. L. Bryden, 1982: Direct estimates and mechanisms of ocean heat transport. *Deep-Sea Res.,* **29,** 339–360.

Hellerman, S., and M. Rosenstein, 1983: Normal monthly wind stress over the World Ocean with error estimates. *J. Phys. Oceangr.* **13,** 1093–1104.

Hogg, N. G., 1994: Observations of Gulf Stream meander-induced disturbances. *J. Phys. Oceanogr.,* **24,** 2534–2545.

Holland, W. R., and F. O. Bryan, 1994: Sensitivity studies on the role of the ocean in climate change. *Ocean Processes in Climate Dynamics: Global and Mediterranean Examples,* P. Malanotte-Fizzoli and A. R. Robinson, Eds., Kluwer, 111–134.

Klinck, J. M., 1995: Thermohaline struture of an eddy-resolving North Atlantic model: The influence of boundary conditions. *J. Phys. Oceanogr.,* **25,** 1174–1195.

Le Dimet, F., and O. Talagrand, 1986: Variational algorithm for analysis and assimilation of meteorological observations: Theoretical aspects. *Tellus,* **38A,** 97–110.

Levitus, S., 1982: *Climatological Atlas of the World Ocean.* NOAA Prof. Paper No. 13, U.S. Govt. Printing Office, 173 pp.

——, 1994a: *World Ocean Atlas 1994.* Vol. 3: *Salinity.* NOAA Atlas NESDIS 3, 99 pp.

——, 1994b: *World Ocean Atlas 1994.* Vol. 4: *Temperature.* NOAA Atlas NESDIS 4, 117 pp.

Lozier, M. S., M. S. McCartney, and W. B. Owens, 1994: Anomalous anomalies in averaged hydrographic data. *J. Phys. Oceanogr.,* **24,** 2624–2638.

Marotzke, J., and C. Wunsch, 1993: Finding the steady state of a general circulation model through data assimilation: Application to the North Atlantic Ocean. *J. Geophys. Res.,* **98,** 20 149–20 167.

Navon, I. M., and D. Legler, 1987: Conjugate-gradient methods for large-scale minimization in meteorology. *Mon. Wea. Rev.,* **115,** 1479–1502.

Oberhuber, J. M., 1988: *An Atlas Based on the COADS Data set: The Budgets of Heat, Buoyancy and Turbulent Kinetic Energy at the Surface of the Global Ocean.* Max-Plank-Institut für Meteorologie, 100 pp.

Roemmich, D., and C. Wunsch, 1985: Two transatlantic sections: Meridional circulation and heat flux in the subtropical North Atlantic Ocean. *Deep-Sea Res.,* **32,** 619–644.

Sasaki, Y., 1970: Some formulations in numerical variational analysis. *Mon. Wea. Rev.,* **98,** 875–883.

Schiller, A., 1995: The mean circulation of the Atlantic Ocean north of 30°S determined by the adjoint method. *J. Mar. Res.,* **53,** 453–497.

——, and J. Willebrand, 1995: A technique for the determination of surface heat and freshwater fluxes from hydrographic observations using an approximation adjoint ocean circulation model. *J. Mar. Res.,* **53,** 433–451.

Schmitt, R. W., P. S. Bogden, and C. E. Dorman, 1989: Evaporation minus precipitation and density fluxes for the North Atlantic. *J. Phys. Oceanogr.,* **19,** 1208–1221.

Schmitz, W. J., Jr., and M. S. McCartney, 1993: On the north Atlantic circulation. *Rev. Geophys.,* **31,** 29–49.

Semtner, A. J., and R. M. Chervin, 1988: A simulation of the global ocean circulation with resolved eddies. *J. Geophys. Res.,* **93,** 15 502–15 522.

Sirkes, Z., and E. Tziperman, 1995: Combining data and a global

primitive equation ocean general circulation model using the adjoint method. *Modern Approaches to Data Assimilation in Ocean Modeling.* P. Malanotte-Rizzoli, Ed., Elsevier Science, 455 pp.

Thacker, W. C., and R. B. Long, 1988: Fitting dynamics to data. *J. Geophys. Res.,* **93,** 1227–1240.

Tziperman, E., W. C. Thacker, R. B. Long, and S. Hwang, 1992a: Oceanic data analysis using a general circulation model. Part I: Simulations. *J. Phys. Oceanogr.,* **22,** 1434–1457.

——, ——, ——, ——, and S. R. Rintoul, 1992b: Oceanic data analysis using a general circulation model. Part II: A North Atlantic model. *J. Phys. Oceanogr.,* **22,** 1458–1485.

Veronis, G., 1975: The role of models in tracer studies. *Numerical Models of the Ocean Circulation,* Natl. Acad. Sci., 133–146.

Yu, L., and J. J. O'Brien, 1995: Variational data assimilation for determining the seasonal net surface heat flux using a tropical Pacific Ocean model. *J. Phys. Oceanogr.,* **25,** 2319–2343.

——, and P. Malanotte-Rizzoli, 1995: Assimilation of North Atlantic climatologies using a primitive equation model—Sensitivity studies. *Proc. Second Int. Symp. on Assimilation of Observations in Meteorology and Oceanography,* Tokyo, Japan, World Meteorological Organization, 565–570.

——, and ——, 1996: Analysis of the North Atlantic climatologies using a combined OGCM/adjoint approach. *J. Mar. Res.,* **54,** 867–913.